

tions should be an important feature of polymer theories attempting to model stresses in extensional flows. We anticipate that the effects of hydrodynamic interactions will be crucial for description of more flexible synthetic polymers such as polystyrene, with a smaller ratio of persistence length to hydrodynamic radius, and hence larger extensibility (L/R_g) ratios.

Finally, conformational hysteresis may play a role in turbulent-drag reduction, an effect discovered by B. A. Toms a half century ago (32): high molecular weight polymers mixed with fluids at an extremely dilute level (~ 1 part per million by weight) can reduce the drag resistance in turbulent flow by as much as 80% (33). Two types of explanations of this effect have been proposed. The first conjecture, originally proposed by Lumley (34), argues that the drag reduction occurs at the boundary between the turbulent-core region and the laminar zone near the pipe surface. Polymers that have been extended by (transient) elongational flows can enter the boundary layer and reduce the momentum transfer between the rapidly moving fluid and the laminar layer. Polymers would remain extended for longer periods of time in their stretched state because of conformational-dependent drag. Hysteresis would further magnify this effect. For synthetic polymers that exhibit a large amount of turbulent-drag reduction, $\zeta^{\text{stretch}}/\zeta^{\text{coil}}$ is estimated to be ~ 18 . In contrast, Tabor and de Gennes have argued (35) that polymers in turbulent flows experience rapidly varying extensional flows so that the coil-stretch transition disappears entirely. Instead, they propose that energy is transferred in turbulent flows through a cascade of eddies to smaller size scales where it is finally dissipated. Long polymers interrupt this cascade by storing some of this energy in the form of an elastic modulus that is then delivered back to the moving fluid.

References and Notes

- R. G. Larson, *The Structure and Rheology of Complex Fluids* (Oxford Univ. Press, New York, 1999).
- H. P. Babcock, R. E. Teixeira, J. S. Hur, E. S. G. Shaqfeh, S. Chu, *Macromolecules* **36**, 4544 (2003).
- R. B. Bird, C. F. Curtiss, R. C. Armstrong, O. Hassager, *Dynamics of Polymeric Liquids* (Wiley, New York, ed. 2, 1987), vol. 2.
- P. G. de Gennes, *J. Chem. Phys.* **60**, 5030 (1974).
- G. G. Fuller, L. G. Leal, *Rheol. Acta* **19**, 580 (1980).
- D. Hunkeler, T. Q. Nguyen, H. H. Kausch, *Polymer* **37**, 4257 (1996).
- M. J. Menasveta, D. A. Hoagland, *Macromolecules* **24**, 3427 (1991).
- E. C. Lee, S. J. Muller, *Macromolecules* **32**, 3295 (1999).
- T. T. Perkins, D. E. Smith, S. Chu, *Science* **276**, 2016 (1997).
- D. E. Smith, S. Chu, *Science* **281**, 1335 (1998).
- E. J. Hinch, in *Proc. Symp. Polym. Lubrification* **233**, 241 (1974).
- R. I. Tanner, *Trans. Soc. Rheol.* **19**, 557 (1975).
- E. J. Hinch, *Phys. Fluids* **20**, s22 (1977).
- Y. V. Brestkin, *Acta Polymerica* **38**, 470 (1987).
- J. J. Magda, R. G. Larson, M. E. Mackay, *J. Chem. Phys.* **89**, 2504 (1988).
- J. M. Rallison, E. J. Hinch, *J. Non-Newtonian Fluid Mech.* **29**, 37 (1988).
- X. J. Fan, R. B. Bird, M. Renardy, *J. Non-Newtonian Fluid Mech.* **18**, 255 (1985).
- J. M. Wiest, L. E. Wedgewood, R. B. Bird, *J. Chem. Phys.* **90**, 587 (1988).
- P. G. de Gennes, *Scaling Concepts in Polymer Physics* (Cornell Univ. Press, Ithaca, NY, 1979).
- F. Reif, *Fundamentals of Statistical and Thermal Physics* (McGraw-Hill, New York, 1965).
- G. K. Batchelor, *J. Fluid Mech.* **44**, 419 (1970).
- We have omitted a numerical constant on the order of unity in this expression.
- D. E. Smith, T. T. Perkins, S. Chu, *Macromolecules* **29**, 1372 (1996).
- T. T. Perkins, D. E. Smith, R. G. Larson, S. Chu, *Science* **268**, 83 (1995).
- DNA molecules were imaged with a Micromax 512BFT camera from Roper Scientific, using a Zeiss Axioplan microscope equipped for epifluorescence with a 40×1.0 numerical aperture objective oil-immersion lens. We used a $0.31\times$ demagnifying lens to provide a field of view of $\approx 480\ \mu\text{m}$. For polymer extensions greater than our field of view, we translated our microscope stage in the direction of molecular stretch to discern total extended lengths. The time scale for translation was on the order of seconds, which was much faster than the time scale of transient molecule dynamics for the range of $\dot{\epsilon}$ probed.
- Materials and methods are available as supporting material on Science Online.
- B. J. Bentley, L. G. Leal, *J. Fluid Mech.* **167**, 219 (1986).
- Polymer relaxation times were measured by first stretching the polymer molecules at high De and then stopping the flow. The extent of the visual image of the molecule is tracked as a function of time, and the final 30% of the relaxation is fit to a decaying exponential $\langle x \cdot x \rangle = A \exp(-t/\tau_x) + B$, where x is dimensional polymer extension, τ_x is the longest polymer relaxation time, and A and B are fitting constants. Observation times $t_{\text{obs}} = \epsilon/\dot{\epsilon}$ on the order of several hours were required for fluid strains of about 10 to 15 units. Therefore, we added a small concentration of Sytox dye (Molecular Probes) to our inlet buffer solutions. Dye molecules bound to DNA exchange with free dye in solution so that fresh dye molecules replenish older, photobleached dye molecules. We also used a mechanical shutter to minimize light exposure from a mercury lamp illuminator and an oxygen-scavenging glucose oxidase-catalase enzyme system to minimize photobleaching. Combining these techniques, we achieved stable polymer relaxation times for at least 7 hours of observation time of a single DNA molecule.
- R. M. Jendrejack, J. J. de Pablo, M. D. Graham, *J. Chem. Phys.* **116**, 7752 (2002).
- C. C. Hsieh, L. Li, R. G. Larson, *J. Rheol.*, in press.
- J. Rotne, S. Prager, *J. Chem. Phys.* **50**, 4831 (1969).
- B. A. Toms, in *Proc. Int. Congr. Rheol.* **2**, 135 (1949).
- P. S. Virk, *Am. Inst. Chem. Eng. J.* **21**, 625 (1975).
- J. Lumley, *J. Polym. Sci. Macromol. Rev.* **7**, 263 (1973).
- P. G. de Gennes, *Introduction to Polymer Dynamics* (Cambridge Univ. Press, Cambridge, 1990).
- We thank M. Gallo and E. Chan at U.S. Genomics for generosity in genomic-length *E. coli* DNA sample preparation and G. Fuller and R. Larson for useful discussions. Supported in part by the Materials Research Science and Engineering Center Program of the NSF (DMR-0213618 and DMR-9808677), the Air Force Office of Scientific Research, and the NSF. C.M.S. was supported in part by an NSF graduate fellowship.

Supporting Online Material

www.sciencemag.org/cgi/content/full/301/5639/1515/DC1

Materials and Methods

SOM Text

Figs. S1 to S3

24 April 2003; accepted 8 August 2003

Electronic Structure Control of Single-Walled Carbon Nanotube Functionalization

Michael S. Strano,^{1*}† Christopher A. Dyke,^{2*} Monica L. Usrey,¹ Paul W. Barone,¹ Mathew J. Allen,² Hongwei Shan,² Carter Kittrell,² Robert H. Hauge,² James M. Tour,^{2,3†} Richard E. Smalley,^{2,4†}

Diazonium reagents functionalize single-walled carbon nanotubes suspended in aqueous solution with high selectivity and enable manipulation according to electronic structure. For example, metallic species are shown to react to the near exclusion of semiconducting nanotubes under controlled conditions. Selectivity is dictated by the availability of electrons near the Fermi level to stabilize a charge-transfer transition state preceding bond formation. The chemistry can be reversed by using a thermal treatment that restores the pristine electronic structure of the nanotube.

The main hurdle to the widespread application of single-walled carbon nanotubes is their manipulation according to electronic structure (1). All known preparative methods (2–4) lead to polydisperse materials of semiconducting, semimetallic and metallic electronic types. Recent advances in the solution-phase dispersion (5, 6), along with spectroscopic identification using band-gap fluorescence (7) and Raman spectroscopy (8), have greatly improved the ability to monitor electrically distinct nanotubes as suspended mixtures and have led to definitive assignments of the optical features of semiconducting (7), as well as metallic and semimetallic, species (8).

We now report selective reaction pathways of carbon nanotubes in which covalent chemical functionalization (9) is controlled by differ-

copy (8), have greatly improved the ability to monitor electrically distinct nanotubes as suspended mixtures and have led to definitive assignments of the optical features of semiconducting (7), as well as metallic and semimetallic, species (8).

We now report selective reaction pathways of carbon nanotubes in which covalent chemical functionalization (9) is controlled by differ-

REPORTS

ences in the nanotube electronic structure. We demonstrate the utility of these chemical pathways for manipulation of nanotubes of distinct electronic types by selective functionalization of metallic nanotubes. This chemistry is a marked departure from previously developed mechanisms for nanotube selectivity that are derived from fullerene chemistry, namely, those based on the carbon pyramidalization angle (10, 11). Controlling nanotube reaction pathways in this way should allow for the separation of semiconducting from metallic and semimetallic nanotubes with high selectivity and scalability, as well as the direct fabrication of devices of a particular electronic type. In contrast to recent work reporting enrichment of metals over semiconductors (12, 13), we show a nearly complete selectivity for particularly metallic species.

The diversity in electronic structure of carbon nanotubes arises from the quantization of the electronic wave vector of the one-dimensional (1D) system through the conceptual rolling of a graphene plane into a cylinder forming the nanotube (2, 4). The vector in units of hexagonal elements connecting two points on this plane defines the nanotube chirality in terms of two integers: n and m . When $|n - m| = 3q$, where q is an integer, the nanotube is metallic or semimetallic, and the remaining species are semiconducting with a geometry-dependent bandgap (14). Although largely unrealized in previous studies, subtle differences in geometric structure of carbon nanotubes lead to marked changes in the rates of solution-phase reactivity of these species. We find that water-soluble diazonium salts (15), which have been shown to react with carbon nanotubes (9, 16, 17), can extract electrons from nanotubes in the formation of a covalent aryl bond (Fig. 1A) and thereby demonstrate highly chemoselective reactions with metallic versus the semiconducting tubes.

This bond forms with extremely high affinity for electrons with energies, ΔE_p , near the Fermi level, E_f of the nanotube (Fig. 1B). The reactant forms a charge-transfer complex at the nanotube surface, where electron donation from the latter stabilizes the transition state and accelerates the forward rate. Once the bond symmetry of the nanotube is disrupted by the formation of this defect, adjacent carbons increase in reactivity (Fig. 1C), and

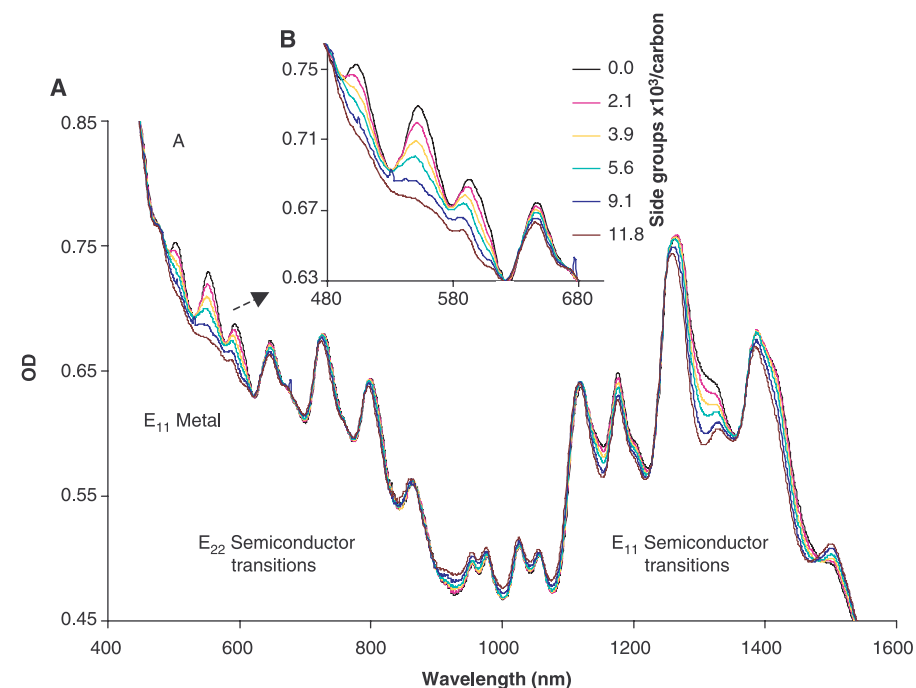
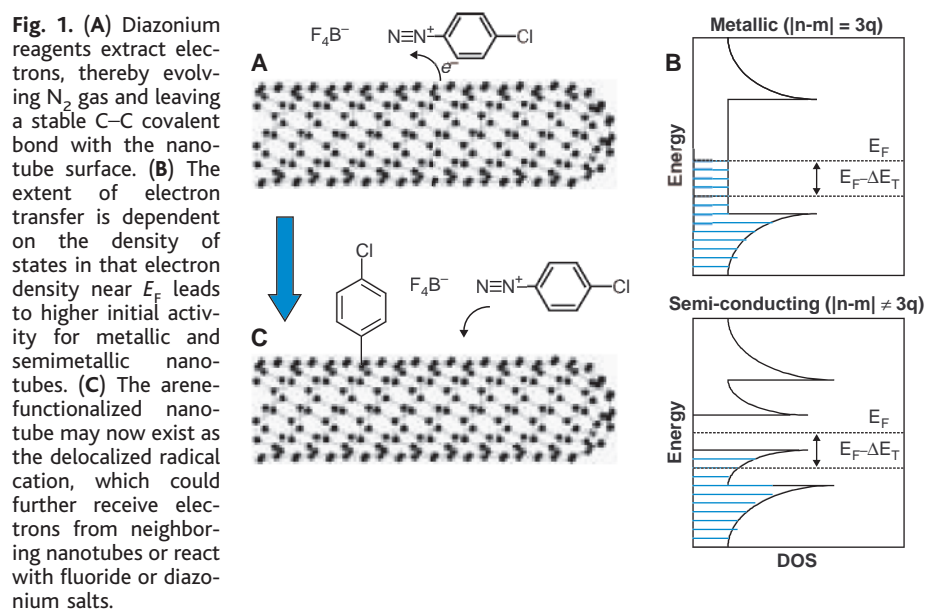


Fig. 2. (A) UV-vis-nIR spectrum of sodium dodecyl sulfate-suspended carbon nanotubes after the addition of various amounts of 4-chlorobenzenediazonium tetrafluoroborate (in mol/1000 mol carbon). Under controlled conditions, semiconductor transitions are unaffected, whereas metals react with high selectivity. (B) Expanded view of the metallic region. The tetrafluoroborate salt causes some bathochromic shifting of the longer wavelength features because of changes in the surfactant adsorbed phase.

the initial selectivity is amplified as the entire nanotube is functionalized.

Under carefully controlled conditions (18), this behavior can be exploited to obtain highly selective functionalization of metallic and semimetallic nanotubes to the exclusion of the semiconductors. Figure 2 shows the ultraviolet-visible-near-infrared (UV-vis-nIR) absorption spectra of aqueous suspended nanotubes after successive additions of 4-chlorobenzenediazonium tetrafluoroborate after steady state. The spectrum monitors the valence (v) to conduction

(c) electronic transitions denoted ($vn \rightarrow cn$) where n is the band index. Figure 2 indicates the $v1 \rightarrow c1$ transitions of the metallic and semimetallic nanotubes from roughly 440 to 645 nm, as well as the $v1 \rightarrow c1$ and $v2 \rightarrow c2$ transitions of the semiconducting nanotubes in the ranges from 830 to 1600 nm and 600 to 800 nm, respectively. These separated absorption features allow for the monitoring of valence electrons in each distinct nanotube; as the species reacts to form covalent linkages, electrons are localized and these maxima decay. Under controlled additions, only

¹Department of Chemical and Biomolecular Engineering, University of Illinois–Urbana/Champaign, Urbana, IL 61801, USA. ²Department of Chemistry, Center for Nanoscale Science and Technology, and Center for Biological and Environmental Nanotechnology, ³Department of Mechanical Engineering and Materials Science, ⁴Department of Physics, Rice University, 6100 Main Street, Houston, TX 77005, USA.

*These authors contributed equally to this work. †To whom correspondence should be addressed. E-mail: strano@uiuc.edu (m.s.); res@rice.edu (R.E.S.); tour@rice.edu (J.M.T.)

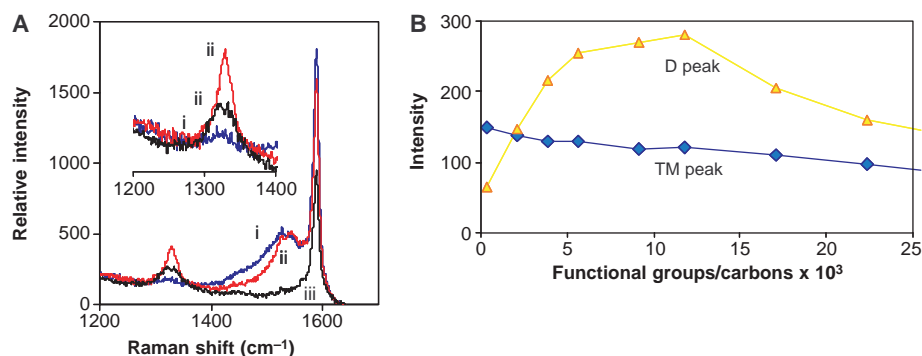


Fig. 3. (A) Raman spectrum at 532-nm excitation, showing the growth of the “disorder” mode with increasing functionalization from 0 (i) to 5.6 (ii) to 22.4 (iii) groups attached per 1000 carbon atoms. (B) The intensity of the tangential mode (TM) $\times 0.1$ decreases as resonance enhancement of the scattering event is lost with increasing reaction. The disorder mode (D) increases sharply then decays because of the same loss of enhancement.

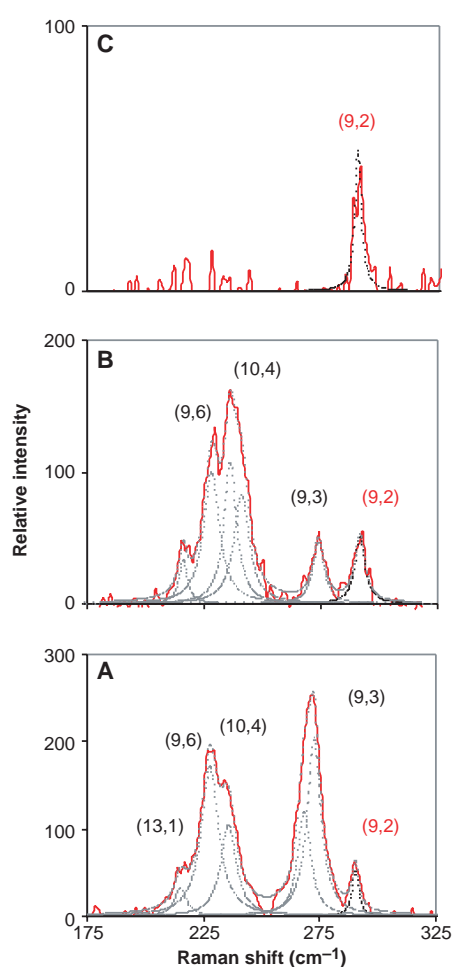


Fig. 4. (A) Low-wave number Raman spectra at 532-nm excitation of the starting solution. Four metallic nanotubes (black) are probed at this wavelength and one semiconductor (red) via a radial mode sensitive to nanotube diameter. (B) After 5.6 groups attached per 1000 carbons, functionalization disrupts this mode, as seen by the decay particularly of the small-diameter metals. This initial evidence of selective reactivity among metals provides a handle for separation of these species. (C) After a ratio of 22.4, all metallic modes have decayed, leaving only the single semiconductor, in agreement with Fig. 2B.

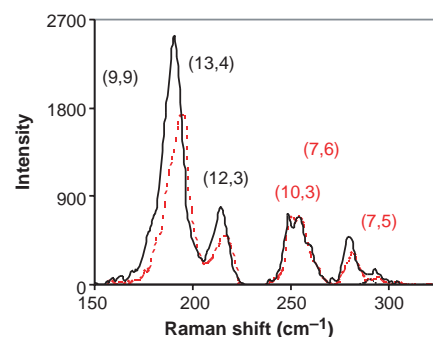


Fig. 5. Raman spectra at 633 nm probing both metals and semiconducting nanotubes before reaction (solid line) and after recovery and thermal pyrolysis (dotted line). The reversibility of the chemistry implies that intrinsic electronic and optical properties of the pristine nanotubes can be recovered.

metallic transitions initially decay (Fig. 2), indicating highly preferential functionalization of metallic nanotubes. This selectivity is remarkable given that these transitions arise from electrons that are much lower in energy compared with the $v1 \rightarrow c1$ and $v2 \rightarrow c2$ transitions of the semiconductors. The selective decay of these metallic transitions is distinct from reversible electronic withdraw (19) or generic “doping” processes (20), as previously reported. Selectivity is also confirmed by the preservation of band-gap fluorescence of the semiconducting nanotubes, which is observed to be highly sensitive to chemical defects. In Fig. 2A, we attribute the change in the feature near 1350 nm to correspond to a nonspecific solvatochromic shift resulting from addition of the BF_4^- counterion that has been observed previously (21).

The functionalization increases the intensity of a phonon mode at 1330 cm^{-1} in the Raman spectrum, as shown in Fig. 3A at 532 nm excitation. Its prominence corresponds with the conversion of an $\text{sp}^2 \text{ C}$ to an $\text{sp}^3 \text{ C}$ on the nanotube during the formation of an $\text{sp}^3 \text{ C-sp}^2 \text{ C}$ nanotube-aryl bond. The so-called D-band involves the resonantly enhanced scattering of an electron via phonon emission by a defect that

breaks the basic symmetry of the graphene plane (2, 4). This peak is not observed to increase as the result of adsorption of hydronium ions (19) or surfactants (5) on the nanotube sidewall. We observe that the height of this peak increases sharply with increasing functionalization, then decreases along with the C-C tangential mode as the system loses electronic resonance (Fig. 3B). These results allow for spectroscopic correlation of the number of sidewall functionalization events to this phonon intensity at low conversion.

The addition of the moiety to the sidewall of the nanotube disrupts the oscillator strength that gives rise to resonantly enhanced, low-frequency Raman lines that are distinct for species of a particular diameter. This causes the mode to decay accordingly as the particular (n,m) nanotube reacts. Figure 4 analogously shows the solution-phase Raman spectra of the mixture at 532 nm with each reactant addition after steady state. The relative rates of the decays of these features reveal unprecedented reactivity differences between chiral semimetallic species. Here, Raman spectroscopy probes nanotubes with nearly identical transition energies, and these differences reveal a curvature-dependent stabilization of the charge-transfer complex that may ultimately be exploited to separate semimetallic and metallic species. When all $v1 \rightarrow c1$ transitions of semimetallic and metallic species have decayed (Fig. 2), only one low-frequency Raman mode that we have previously assigned to the (9,2) semiconductor (19) remains unaffected. These results also independently confirm the recent spectroscopic assignment of these features (7, 8).

Carbon nanotube chemistry has been correctly described with a pyramidization angle formalism (10). Here, chemical reactivity and kinetic selectivity are related to the extent of s character due to the curvature-induced strain of the sp^2 -hybridized graphene sheet. Because strain energy per carbon is inversely related to nanotube diameter, this model predicts that smaller diameter nanotubes will be the most reactive, with the enthalpy of reaction decreasing as the curvature becomes infinite. Although such behavior is most commonly the case, our findings underscore the role of electronic structure in determining the reactivity of the nanotube. Because such a structure is highly sensitive to chiral wrapping, chemical doping, and charged adsorbates, as well as to nanotube diameter, there is a considerable diversity of these various pathways, in addition to a simple diameter dependence.

Thermal pyrolysis of the reacted material at 300°C in an atmosphere of inert gas cleaves (22) the aryl moieties from the sidewall and restores the spectroscopic signatures of the aromatic, pristine nanotubes (9). Figure 5 compares the Raman spectra before and after recovery and thermal pyrolysis at 633 nm (Fig. 5). This wavelength was used because it probes a mixture of metals and semiconductors for samples prepared by CO disproportionation (8). The radial phonon

modes are nearly completely restored after thermal treatment. Similarly, electronic transitions in the absorption spectrum are restored, indicating the loss of the side group and a restoration of the original electronic structure of the nanotube (22). Hence, this selective chemistry can be used as a reversible route to separate, deposit, or chemically link nanotubes of a particular electronic structure, and the original optical and electronic characteristics can then be recovered.

References and Notes

- P. Avouris, *Acc. Chem. Res.* **35**, 1026 (2002).
- M. S. Dresselhaus, G. Dresselhaus, P. C. Eklund, *Science of Fullerenes and Carbon Nanotubes* (Academic Press, San Diego, CA, 1996).
- M. J. Bronikowski, P. A. Willis, D. T. Colbert, K. A. Smith, R. Smalley, *J. Vac. Sci. Technol.* **19**, 1800 (2001).
- R. Saito, G. Dresselhaus, M. S. Dresselhaus, *Physical Properties of Carbon Nanotubes* (Imperial College Press, London, 1998).
- M. S. Strano *et al.*, *J. Nanosci. Nanotechnol.* **3**, 81 (2003).
- M. J. O'Connell *et al.*, *Science* **297**, 593 (2002).
- S. M. Bachilo *et al.*, *Science* **298**, 2361 (2002).
- M. S. Strano, *Nanoletters* **3**, 1091 (2003).
- J. L. Bahr, J. M. Tour, *J. Mater. Chem.* **12**, 1952 (2002).
- S. Niyogi *et al.*, *Acc. Chem. Res.* **35**, 1105 (2002).
- Z. F. Chen, W. Thiel, A. Hirsch, *Chemphyschem* **4**, 93 (2003).
- M. Zheng *et al.*, *Nature Mater.* **2**, 338 (2003).
- D. Chattopadhyay, I. Galeska, F. Papadimitrakopoulos, *J. Am. Chem. Soc.* **125**, 3370 (2003).
- S. Reich, C. Thomsen, *Phys. Rev. B* **62**, 4273 (2000).
- C. Bravo-Diaz, M. Soengas-Fernandez, M. Rodriguez-Sarabia, E. Gonzalez-Romero, *Langmuir* **14**, 5098 (1998).
- C. A. Dyke, J. M. Tour, *J. Am. Chem. Soc.* **125**, 1156 (2003).
- J. L. Bahr *et al.*, *J. Am. Chem. Soc.* **123**, 6536 (2001).
- A recirculating flow reactor was used to transfer sodium dodecyl sulfate-suspended carbon nanotubes at pH = 10 at a flow rate of 150 ml/min through a cuvette with inlet and outlet ports. Continuous UV-vis-NIR spectra were generated after the addition of a metered amount of diazonium aryl chloride tetrafluoroborate. Additions were made in 0.05 mM increments after the system had reached steady state.
- M. S. Strano *et al.*, *J. Phys. Chem. B* **107**, 6979 (2002).
- M. E. Itkis *et al.*, *Nanoletters* **2**, 155 (2002).
- Increasing the ionic strength of the surfactant-suspended nanotubes screens the charged repulsion of the sulfate head groups and causes the adsorbed layer to adopt a configuration that allows greater access of water to the surface. This causes a characteristic red shift of the absorption transitions that is most prominent for the $v_1 \rightarrow \pi^*$ transitions of the semiconductors. Because of the convolution of the transitions in the spectrum, this shifting is seen as a change in intensity of one region in particular. The results can be qualitatively duplicated by the addition of 100 mM NaCl to the solution.
- Thermogravimetric analysis, as well as absorption and Raman spectra of the reacted and thermally restored material, are available as supporting material on Science Online.
- We thank J. White for assistance with Raman spectroscopy. M.S.S. acknowledges the financial support of the University of Illinois, School of Chemical Sciences. Support at Rice University was provided by the NSF Focused Research Group on Fullerene Nanotube Chemistry (DMR-0073046), the NSF Center for Biological and Environmental Nanotechnology (EEC-0118007), NASA URETI NCC-01-0203, Air Force Office of Scientific Research (F49620-01-1-0364), and the Office of Naval Research Polymer Division. Support from NASA (NCC9-77) for development of the HiPco method is also gratefully acknowledged.

Supporting Online Material

www.sciencemag.org/cgi/content/full/301/5639/1519/DC1
Materials and Methods
Figs. S1 to S3

5 June 2003; accepted 5 August 2003

Anomalous Nitrogen Isotope Ratio in Comets

Claude Arpigny,^{1*} Emmanuël Jehin,² Jean Manfroid,¹
Damien Hutsemékers,¹ Rita Schulz,³ J. A. Stüwe,⁴
Jean-Marc Zucconi,⁵ Ilya Ilyin⁶

High-resolution spectra of the CN $B^2\Sigma^+ - X^2\Sigma^+$ (0,0) band at 390 nanometers yield isotopic ratios for comets C/1995 O1 (Hale-Bopp) and C/2000 WM1 (LINEAR) as follows: 165 ± 40 and 115 ± 20 for $^{12}\text{C}/^{13}\text{C}$, 140 ± 35 and 140 ± 30 for $^{14}\text{N}/^{15}\text{N}$. Our N isotopic measurements are lower than the terrestrial $^{14}\text{N}/^{15}\text{N} = 272$ and the ratio for Hale-Bopp from measurements of HCN, the presumed parent species of CN. This isotopic anomaly suggests the existence of other parent(s) of CN, with an even lower N isotopic ratio. Organic compounds like those found in interplanetary dust particles are good candidates.

Determination of the abundance ratios of the stable isotopes of the light elements in different objects of the solar system (SS) provides important clues regarding origin of the SS and its early history. Comets are among the best-preserved specimens of the primitive solar nebula and, as such, they can play an outstanding role. The ground-based determination of their C and N isotope ratios is based on the comparison of the intensities of spectral features of the various isotopic species. The observed molecules are CN and C_2 in the optical domain and HCN in the submillimeter range. These measurements are difficult in both domains due mainly to the weakness of the emissions of the low-abundance species (1).

We observed comet C/2000 WM1 (hereafter designated as "WM1") in March 2002 with the Ultraviolet-Visual Echelle Spectro-

graph (UVES) (2) mounted on the 8.2-m UT2 (Kueyen) telescope of the European Southern Observatory Very Large Telescope (ESO VLT) array at Cerro Paranal, Chile, in order to measure the C and N isotopic ratios from the CN Violet (0,0) band (Fig. 1).

Cometary emissions are produced by absorption of the solar light followed by re-emission of lines of different frequencies, a process called resonance-fluorescence. The synthetic fluorescence spectra of the various isotopomers $^{12}\text{C}^{14}\text{N}$, $^{13}\text{C}^{14}\text{N}$, and $^{12}\text{C}^{15}\text{N}$ ($^{13}\text{C}^{15}\text{N}$ is negligible) were computed for each observing circumstance (Table 1) (3) according to the scheme described by Zucconi and Festou (3). The isotope ratios are estimated by fitting the average observed CN spectrum with a linear combination of the synthetic spectra of the three species (3). The final values are $^{12}\text{C}/^{13}\text{C} = 115 \pm 20$ and $^{14}\text{N}/^{15}\text{N} = 140 \pm 30$ (Fig. 2). The "errors" cited give the deviations of the values for which acceptable fits are obtained using various procedures and various sets of lines (3). These ratios are consistent with estimates of Hale-Bopp in which we identified the presence of $^{12}\text{C}^{15}\text{N}$ (4) and for which we have now derived $^{12}\text{C}/^{13}\text{C} = 165 \pm 40$ and $^{14}\text{N}/^{15}\text{N} = 140 \pm 35$.

The C ratio was measured in situ by the VEGA and GIOTTO spacecraft in P/Halley (5) and from ground-based, submillimeter,

¹Institut d'Astrophysique et de Géophysique, Sart-Tilman, Bâtiment B5c, B-4000 Liège, Belgium. ²European Southern Observatory, Casilla 19001, Santiago, Chile. ³ESA/RSSD, ESTEC, Post Office Box 299, NL-2200 AG Noordwijk, Netherlands. ⁴Leiden Observatory, NL-2300 RA Leiden, Netherlands. ⁵Observatoire de Besançon, F25010 Besançon Cedex, France. ⁶Astronomy Division, Post Office Box 3000, FIN 90014 University of Oulu, Finland.

*To whom correspondence should be addressed. E-mail: Claude.Arpinig@ulg.ac.be

Fig. 1. The UVES average observed spectrum (1) of the R branch of the CN (0,0) band in comet C/2000 WM1. Some of the rotational lines are labeled with the quantum number N of the lower level of the corresponding transition. The small features between the R lines are essentially P lines of the (1,1) band. "Hidden" among these lines, at a still smaller level, are the R lines of $^{12}\text{C}^{15}\text{N}$ and $^{13}\text{C}^{14}\text{N}$.

